[redacted]

576

VOYAGER 1 AND 2

PLASMA JUPITER ANALYZED DATA

77-084A-06C, 77-076A-06C

VOYAGER 1 & 2

JUPITER PLASMA DATA TAPE

77-084A-06C

77-076A-06C

THESE DATA SETS HAVE BEEN RESTORED. ORIGINALLY THEY CONTAINED ONE 9-TRACK, 6250 BPI TAPE WRITTEN IN BINARY. THERE IS ONE RESTORED TAPE. THE DR TAPE IS A 3480 CARTRIDGE AND THE DS TAPE IS 9-TRACK, 6250 BPI. THE ORIGINAL TAPE WAS CREATED ON AN IBM 360 COMPUTER AND WAS RESTORED ON AN IBM 9021 COMPUTER. THE DR AND DS NUMBER ALONG WITH THE CORRESPONDING D NUMBER AND TIME SPAN IS AS FOLLOWS:

DR#	DS#	D#	FILES	TIME SPAN
DR005307	DS005307	D056366	1	03/01/79 - 03/07/79 VOY 1
			2	07/04/79 - 07/12/79 VOY 2

REQ. AGENT	REQ. NO.	ACQ. AGENT
DEW	V0178	RWV

VOYAGER 1 AND 2

PLASMA JUPITER ANALYZED DATA

77-084A-06C, 77-076A-06C

THIS DATA SET CATOLOG CONSISTS OF 1 TAPE. THE TAPE IS 6250 BPI, 9 TRACK, BINARY , WITH 2 FILES OF DATA. THE TAPE WAS CREATED ON AN IBM COMPUTER. THE D AND C NUMBERS ARE AS FOLLOWS:

D#	C#	TIME SPAN
D-56366	C-23055	3/1/79-3/7/79 (FILE 1) 7/4/79-7/12/79 (FILE 2)

MASSACHUSETTS INSTITUTE OF TECHNOLOGY
CENTER FOR SPACE RESEARCH
CAMBRIDGE, MASSACHUSETTS 02139

37-695
(617) 253-4285

January 18, 1983

Ms. Winifred Cameron
National Space Science Data Center
Acquisition and Analysis Branch
Code 601.1
Greenbelt, Maryland 20771

Dear Ms. Cameron:

As per our phone conversation of last week, I am submitting to the NSSDC a magnetic tape containing analyzed plasma parameters derived from data for the Plasma Science Experiment on Voyagers 1 and 2, during the Jupiter encounters. These analysis parameters characterize the low-energy plasma environment (<6 kV) in the Jovian magnetosphere. Professor H. S. Bridge is the Principal Investigator. Appropriate documentation for this tape is enclosed.

If you have any questions, please call me at the above number.

Sincerely yours,

John W. Belcher
Professor of Physics

JWB/ab
Enclosure

77-084A-06C
77-076A-06C

Voyager Plasma Science Analysis Tape

Jupiter Encounters

H. S. Bridge

Principal Investigator

Submitted by: J. W. Belcher

Department of Physics and

Center for Space Research

Massachusetts Institute of Technology

Cambridge, Massachusetts 02139

January, 1983

Table of Contents

I. Science Rationale

The Voyager Plasma Science Experiment (PLS) is designed to measure the properties of interplanetary and magnetospheric plasmas with energies per charge between 10V and 5950V, for both electrons and positive ions (Bridge et al., 1977). The analysis and data described herein pertain to the magnetospheric measurements obtained during the Jupiter encounters of Voyager 1 and Voyager 2. Previous to the Voyager encounters, little was known about the properties of the low-energy plasma in the Jovian magnetosphere, and the data gathered by PLS represent a significant advance in our knowledge of the Jovian magnetosphere. Publications growing out of this data set are listed in the bibliography. Some of the major results of the investigation were: (1) measurements of positive-ion properties in the Io plasma torus and inner to middle magnetosphere of Jupiter (i.e., densities, temperatures, composition, with some velocity information); (2) measurements of magnetospheric electron properties from the Io plasma torus to the outer magnetosphere; (3) discovery of the breakdown of rigid corotation in the middle magnetosphere; and (4) direct measurements of the velocity perturbations associated with the Alfvén wave generated by Io. A comprehensive review of the PLS results at Jupiter is given in Belcher (1982), and the naive user should start with this article (copies are available upon request from MIT).

II. Instrument Description

The Plasma Science Experiment is well-described in the literature (Bridge et al., 1977), and we give only a brief description here. The Plasma Science experiment consists of four modulated-grid Faraday cups, three of which (A, B, C) are symmetrically positioned about an axis that generally points toward the

Earth, and a fourth (the side sensor, D) oriented at right angles to this direction. Positive-ion measurements are made in all four sensors, and electron measurements in the D sensor alone. We first discuss the positive ion measurements.

A. Positive-Ion Measurements

Each of the four PLS sensors provides an energy-per-charge scan of the positive-ion plasma between 10 and 5950V. The scan in velocity space is integral in the directions perpendicular to the sensor normal and differential in the direction in velocity space along the sensor normal. Thus the four energy-per-charge scans provide reduced one-dimensional ion distribution functions for four different directions in velocity space, convolved with the response functions of the sensors (see Appendix A of McNutt, Belcher, and Bridge, 1981).

Figure 1 shows the Voyager trajectory projected onto the Jovian equatorial plane. Also shown is the projection of the symmetry axis of the main sensor cluster (S), which consists of the A, B, and C cups. The projection of the normal of the side-looking sensor, the D cup, is also indicated (D). The prime field of view of the main cluster is roughly a cone of half-angle 45° about the symmetry axis, and the field of view of the side sensor is a cone of half-angle 30° about the cup normal. It is apparent from this figure that plasma corotating with Jupiter will flow into the D sensor over most of the inbound leg of the trajectory. Cold corotating flow moves out of the D sensor and into the field of view of the main cluster near closest approach, and out of the field of view of all sensors on the outbound leg. Thus, on Voyager 1, positive-ion data are obtained primarily from inbound observations; in the torus proper, the data come from the three Faraday cups in the main cluster, whereas in the middle magnetosphere (outside of 10 R_J), they are

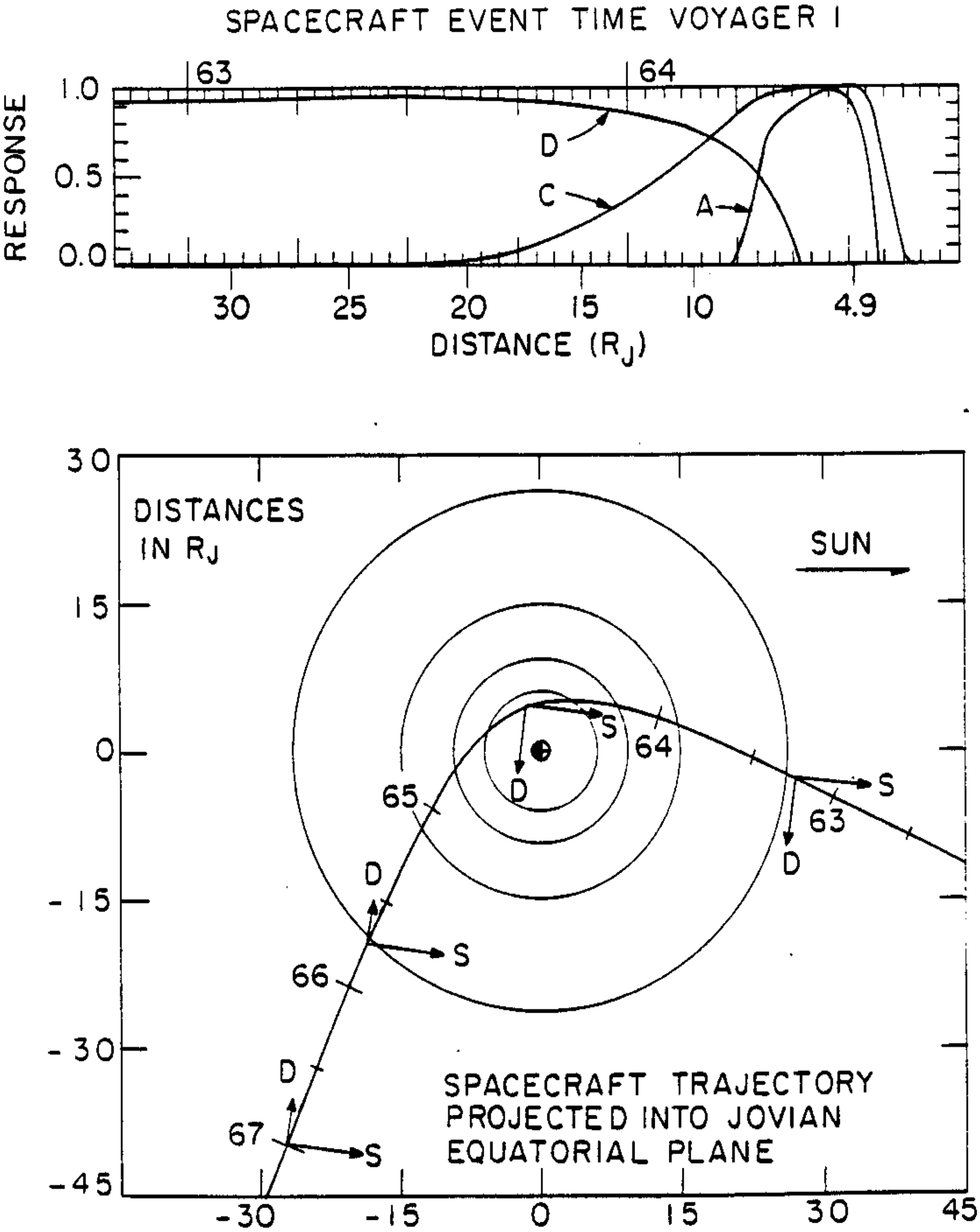

Fig. 1. The Voyager 1 trajectory projected onto the Jovian equatorial plane. The arrow labeled S is the projection of the symmetry axis of the main cluster of Faraday cups onto the equatorial plane, and the arrow labeled D is the projection of the D cup axis. On the inbound leg the A and D cup axes are essentially in the Jovian equatorial plane, with the B and C cup axes inclined -17° south and north of that plane, respectively. Tick marks are shown every 12 hours, with day of the year at the beginning of the day. The orbits of the four Galilean satellites are also shown. The top panel shows the response of three of the sensors to a cold, corotating beam, as a function of time along the trajectory. Closest approach is at 4.9 R_J (1204 UT on DOY 64, 1979).

obtained primarily from the side sensor. The positive ions are generally transonic to highly supersonic. Because of the unfavorable look directions, positive-ion data outbound are thus of much poorer quality than inbound. During the Voyager 2 encounter, the viewing geometry was similar to that of Voyager 1, but the closest approach distance of 10 R_J precluded observations in the torus.

There are two positive-ion measurement modes: a low resolution energy-per-charge mode (the "L" mode), with 16 energy channels between 10V and 5950V; and a high resolution energy-per-charge mode (the"M" mode), with 128 steps between 10V and 5950V. In general, the L mode is most useful in the outer and middle magnetosphere because of its high signal-to-noise ratio, whereas the M mode is crucial for composition studies in the middle and inner magnetosphere. Figure 2 shows an M mode measurement in the D sensor in the middle magnetosphere, exhibiting some of the heavy ion peaks characteristic of of the Jovian plasma (H^+, O^{2+}, S^{3+}, O^+ or S^{2+}, Na^+, S^+ (not shown in this figure)). In the analysis results described below, we use the terms "moments" and "fits". A moment analysis does not assume a particular form for the positive- ion distribution function, or a composition, but instead is a simple sum over the observed distribution function. For example, the area under the curve in Figure 2 is a measure of the total positive-ion charge density, and is straightforward to compute in either the L or M mode. In the Description of Analysis Records, Section III, the term "moment density" refers to such simple sums. On the other hand, we can also fit each of the peaks in Figure 2 to a Maxwellian, and thus arrive at parameters describing the density, temperature, etc., of each of the heavy ion components. Such parameters are referred to as "fit" parameters. In general, a moments analysis can always be done, whereas a fit analysis requires that the plasma be cold in some sense. Thus the fit

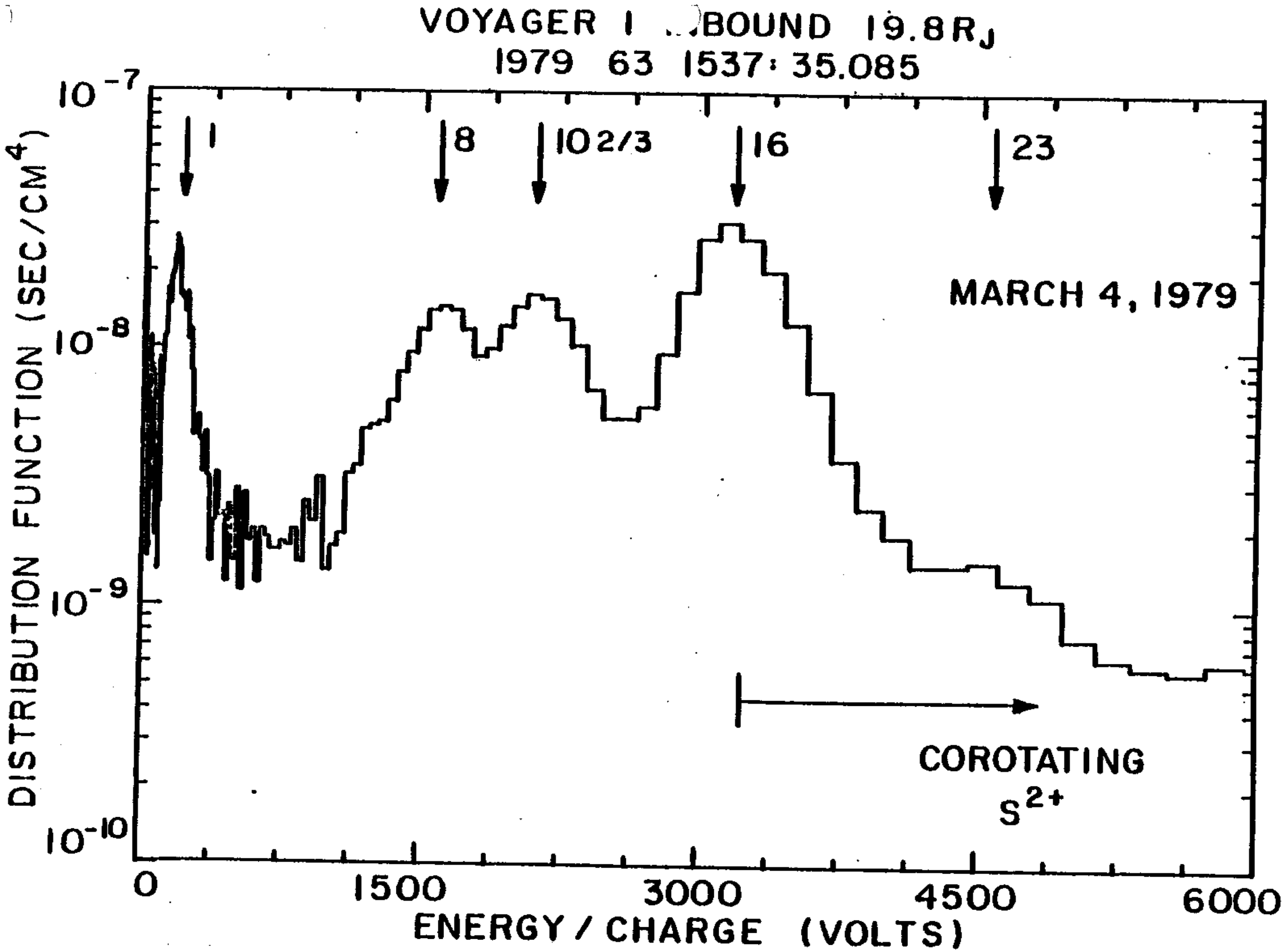

Fig. 2. A high resolution M-mode measurement from the D sensor of the positive-ion distribution function at 19.8 R_J. A least squares fit to the 8, 10-2/3, and 16 peaks yields a common velocity component of 195 km/sec into the D sensor, and this velocity is used to draw the various arrows in the figure. The velocity component expected on the basis of rigid corotation is 238 km/sec. The expected energy-per-charge of an S^{2+} ion moving at the rigid corotation speed is indicated.

analyses are much more sparse than the moment analyses (see the discussion in McNutt et al. (1981)).

B. Electron Measurements

In some respects (e.g., spacecraft charging effects), the electron analysis is much more complex (Scudder et al., 1981) than the positive-ion analysis. In other respects it is less complex (i.e., there is only one species of electron, and the electrons are always highly subsonic). There are two modes for electron measurements: the low energy electron mode (E1), with 16 energy steps between 10V and 140V, and the high energy electron mode (E2) with 16 energy steps between 10V and 5950V. In the electron analysis, the two electron modes (E1 and E2) are combined to arrive at a complete electron energy spectrum. Such spectra are shown in Figure 3. In general, these spectra exhibit a cold Maxwellian "core" component and a hot suprathermal "halo" component. In the electron analysis, as in the ion analysis, there is a "moment" analysis and a "fit" analysis, with the same meaning. The "fit" is to two Maxwellians, one hot and one cold.

C. Mode Timing

The integration time for a given energy channel is 240 milli-seconds. Thus it takes 30.72 seconds to take a full M mode (128 steps), and 3.84 seconds each to take an E1, E2, and L mode (16 steps). The spectra are taken in the sequence M, E1, L, E2. Times associated with a given mode are beginning times of the mode. An entire M, E1, L, E2 sequence takes 96 seconds to complete. However, a complete M mode is not telemetered every 96 seconds. We send the first 72 channels of the 128 steps from one 96-second sequence, and then the last 72 channels from the next 96-second sequence. Thus, it takes 192 seconds to get a complete M mode. In the M-mode analysis, two each 96 seconds the data are "updated" with the latest 72 channels measured.

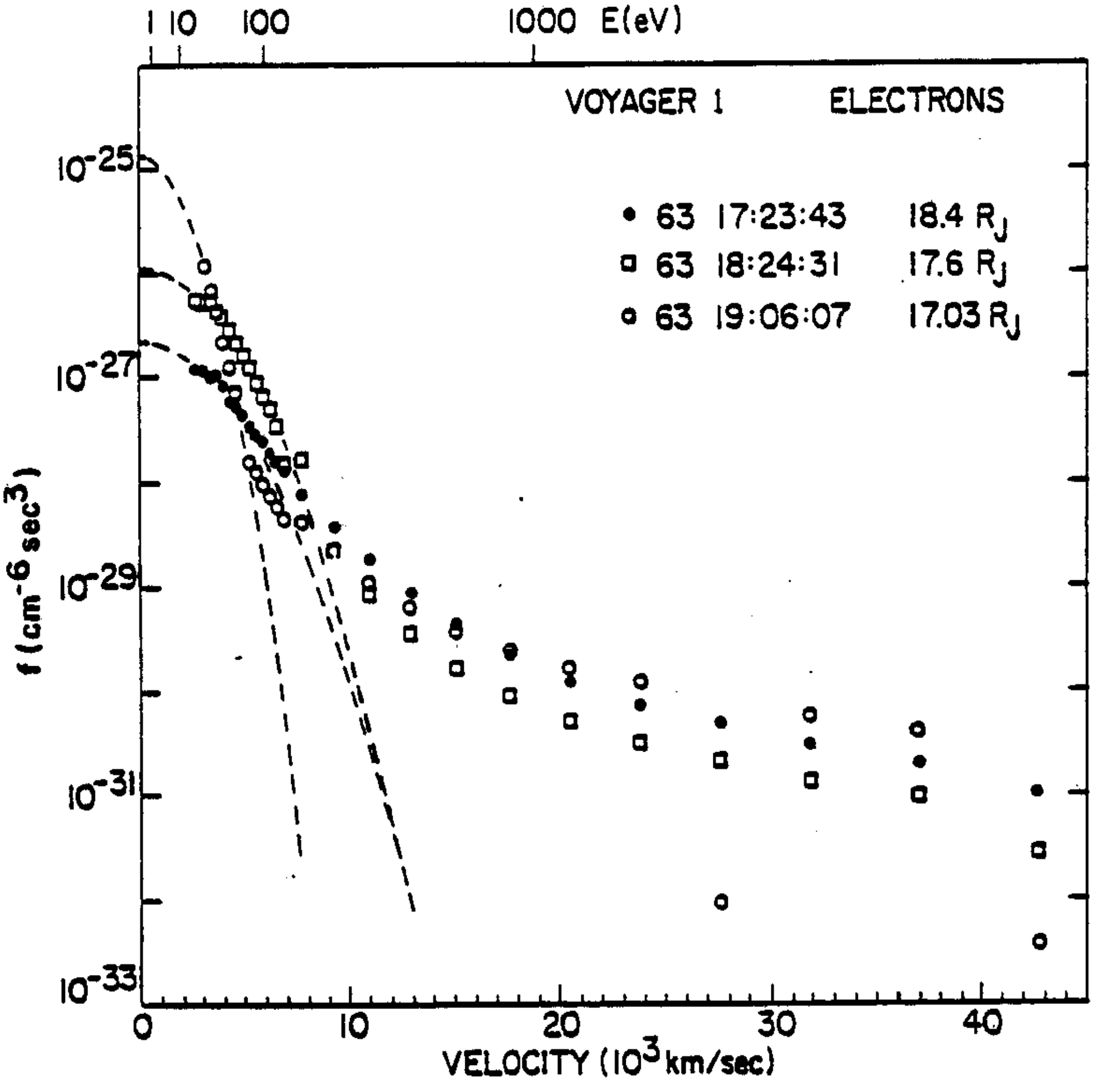

Fig. 3. Electron distribution functions versus electron speed during the Voyager 1 inbound plasma sheet crossing near 17 R_J. For reference, the corresponding electron energy in eV is given at the top of the figure. Gaussian fits to the cold "core" electron component are indicated by the dashed lines.

III. Description of the Analysis Records

There are seven different types of records on the Plasma Science Analysis Tapes. Each type is read by an identical statement, i.e.,

```
DIMENSION JTIME(6), A(30)
READ(10) JTIME,JMOD,JCAT,JGEN,A
```

The array JTIME always contains (year, day, hour, minute, sec, millisec) in I*4. Time always increases or stays the same (if we are analyzing the same spectrum two different ways, for example). The I*4 variable JMOD identifies the data mode (JMOD=1, 2, 3 refers to L-mode data, M-mode data, and electron mode data, respectively). The I*4 variable JCAT refers to the type of analysis on that data, and JGEN is a generation date (month day year in one I*4 variable). The matrix A (REAL*4) contains the results of the analysis. Exactly what is contained in A will depend on the mode and type of analysis, as we describe below for each of the seven types of records. In general, the positive-ion moment analysis is in a different type of record than the fit analysis (values of JCAT differ). For the electrons, however, the fit and moment analysis are contained in the same type of record. All fill values are Z7FFFFFFF.

A. L-Mode Positive-Ion Charge Densities, Moment (JMOD=1,JCAT=1).

These types of records are moment analyses (JCAT=1) of L-mode data (JMOD=1). They also contain some trajectory and magnetic field data. The purpose of the moment analysis is to provide an estimate of the positive-ion charge density, N_+, in elementary charges per cubic centimeter, and of the positive ion mass density, N_m, in amu per cubic centimeter. The estimates of N_+ are reliable, subject to the caveats below. The estimates of N_m, on the other hand, are unreliable for a variety of reasons, and should be ignored.

The moment charge density N_+ is computed as follows. Let V_n be the component of plasma velocity into a given sensor. Assume that there are M positive-ion species, each with density N_i, mass number A_i and charge number Z_i, i = 1,2,...M. Let I_j be the current in the j-th channel of a positive-ion mode (L or M) and A_{eff} the effective area of the cup. Then as shown in Appendix A of McNutt et al. (1981), a good estimate of N_+ for a cold beam is

$$N_+ = \Sigma_i Z_i N_i = \Sigma_j I_j/(eA_{eff}V_n)$$

Provided that we have an estimate of V_n from other sources, we can estimate N_+, even though individual ion peaks are not resolved.

The definition of the elements of the answer array are as follows:

A(1): radial distance of the s/c from Jupiter, in Jovian radii ($1\ R_J$ = 71,372 km), at the beginning time of the mode.

A(2): System III latitude of the s/c, degrees

A(3): System III longitude of the s/c, degrees

A(4): Cup number from which moment density derived (1,2,3,4 is A,B,C,D cup). This is 4 in the middle magnetosphere, switching to 1,2, or 3 near closest approach. For analysis, we chose that cup which has maximum response to a cold corotating beam.

A(5): Response r of the chosen cup to a cold corotating cold beam ($0. \leq r \leq 1.$, and r is 1. at normal incidence).

A(6): Component of properly aberrated rigid corotation velocity into the chosen cup, in km/sec.

A(7): Estimate of N_+ from equation (1), using rigid corotation for an estimate of V_n (from A(6)), with $A_{eff} = 64.8\ cm^2$ for the main cluster ($1/eA_{eff} = 9.633 \times 10^{-4}$ for I; in femtoamps and V_n in km/sec) and $A_{eff} = 68$ cm^2 for the side sensor ($1/eA_{eff} = 9.179 \times 10^{-4}$).

A(8): Estimate of $N_m = \Sigma A_i N_i$, not reliable.

A(9): Estimate of solar wind or magnetosheath proton density from A cup of main sensor, computed using standard solar wind scheme (Bridge et al., 1977). Not useful in the magnetosphere.

A(10): Gain state of the instrument (not useful to the general user)

A(11): Capacitor state (not useful)

A(12): Conversion factor from digital numbers to femtoamps (not useful).

A(13): Cylindrical radial component of magnetic field at the time of peak current in this positive-ion spectrum.

A(14): Cylindrical azimuthal component of magnetic field.

A(15): Cylindrical z component of magnetic field, where z-axis is parallel to Jovian rotation axis.

A(16): Fill (Z7FFFFFFF)

A(17): Number of current channels used in computing density in sum of equation (1).

A(18): → A(30): Fill (Z7FFFFFFF)

Caveats on Use: The estimates of N_+ are subject to the general systematic errors enumerated in McNutt et al. (1981), page 8324). In particular, in the outer magnetosphere, the hot suprathermal electrons cause an electron feed-through into the positive ion measurements, contaminating estimates of N_+ in that region. An estimate of the amount of contamination can be obtained from the electron records (see III G, below).

In addition, we note that the estimate of N_+ in A(7) in this type of record <u>differs</u> from the published curves in Figure 6 and 7 of McNutt et al. (1981), as follows. On this tape, we have assumed V_n is rigid corotation everywhere, whereas McNutt et al. (1981) assume V_n is rigid corotation inside of 17.5 R_J, and 200 km/sec into the D sensor outside of 17.5 R_J (see p. 8323). The values of McNutt et al. (1981) can easily be obtained from the present values by multiplying A(7) by A(6)/200 outside of 17.5 R_J inbound. L-mode estimates of N_+ should not be used inside of 15 R_J, if they are smaller than M-mode estimates inside of 15 R_J, as the L-mode saturates near closest approach. Instead, the M-mode estimates should be used (see below). However, L-mode estimates should always be used in preference to M-mode estimates outside of 15 R_J, because of signal-to-noise problems in the M-mode. Since the publication of the McNutt et al. (1981) paper, a better value of A_{eff} for the side (main) sensors has been determined to be 56.2 (67.4) cm^2. Thus the moment densities on this tape should be multiplied by a factor of 1.21 (1.04) for estimates derived from the side (main) sensors.

Finally, we note that the field data here are to be regarded as diagnostic only, in that they were derived from early versions of the field analysis. The definitive source of field data is the Summary tapes submitted to NSSDC by the magnetometer team.

B. <u>M-mode Positive-Ion Charge Densities, Moment (JMOD=2, JCAT=1)</u>

These estimates of N_+ are calculated exactly as above, using the high resolution M-mode instead of the low resolution L-mode. The answer array A has the same meaning as above. Again, note that M-mode densities are subject to higher signal-to-noise outside of ~15 R_J, and the L-mode is preferable. Inside 15 R_J, the L-mode sometimes saturates, and the M-mode estimate is preferable.

C. Selected Middle Magnetosphere L-mode Fits, McNutt (JMOD=1,JCAT=2)

As discussed in detail in McNutt et al. (1981, p. 8325), L-mode fits are possible when the H^+ peak is well resolved from the heavy ion peak. For these resolved L-mode spectra, McNutt et al. (1981) fit H^+, S^{3+}, and O^+, with S^{3+} and O^+ constrained to have the same temperature, and H^+ an independent temperature. All species are assumed to be comoving. This record type contains information on these fits, with information in the answer array defined as follows, for the I-th positive-ion species (I=1,2,3).

IA = 8 * (I-1)

A(1 + IA): fit density of the I-th species, number/cc

A(2 + IA): uncertainty in density, fraction

A(3) + IA): fit velocity component into the D-sensor (same for all species), in km/sec

A(4 + IA): uncertainty in velocity component, fraction

A(5 + IA): fit thermal speed for the I-th species, in km/sec

A(6 + IA): uncertainty in thermal speed, fraction

A(7 + IA): mass number for I-th species

A(8 + IA): charge number for I-th species

A(25): $\log_{10}$ of the χ^2 of the fit

A(26): Alfven velocity, km/sec

A(27): mass density, amu/cc

A(28): guess for proton density based on three channels, number/cc

A(29): guess for proton velocity component, km/sec

A(30): guess for proton thermal speed, km/sec

The last three elements of the answer array above are estimates of proton parameters based on the proton peak and two adjacent channels, and are used as a starting point for the non-linear least squares fit. Note that this is a simultaneous fit to the proton and heavy ion peaks.

Caveats on Use: In the L-mode, the fits are considered "bad" if the Mach number of the protons (A(3)/A(5)) is less than 1.16, or if the fractional error in velocity isgreater than 0.2, or if the Mach number of the S^{3+} is less than 1.0. The density estimates here are low for the reasons discussed in III A above, and should be multiplied by 1.21, as these fits are all derived from D-sensor data.

D. Selected Middle Magnetosphere M-mode Fits, McNutt (JMOD=2, JCAT=2)

McNutt et al. (1981) selected ~60 "high-quality" M-mode spectra which were cold enough so that three heavy ion peaks were well-resolved. These spectra were fit assuming that the three heavy ion peaks were O^{2+}, S^{3+}, and O^{+}. No proton parameters appear in these fits. Each of the three has independent density and thermal speed; all three species are assumed to have a common velocity. The answer array is as defined in III C above, except that A(28 → 30) is fill (no proton parameters)

Caveats in Use: In the M-mode, the fits are considered "bad" if the fractional error in velocity is greater than 0.2, or if the Mach number of the S^{3+} is less than 1.0. The density estimates here are again low as in III A above, and should be multiplied by 1.21 (all D-sensor data).

E. Continuous Middle Magnetosphere M-mode Fits, McNutt (JMOD=2, JCAT=5)

For a brief period of time on Voyager 1 (March 4, 1700 to March 5, 0500), McNutt has run fits to all M-mode, D-sensor spectra, whether or not resolved heavy-ion peaks are present. The fits are as in III D above, with the same meaning for the answer array.

Caveats in Use: Velocity components into the D-sensor are suspect because of the lack of resolved peaks. These fits should be taken as qualitative only.

F. Io Torus M-mode Fits, Bagenal (JMOD=2,JCAT=3 and 4)

All fits discussed above have been to the D-sensor. In the inner magnetosphere, corotating flow is into the main sensor, and Bagenal and Sullivan (1981) have performed a number of fits of various positive-ion species to data taken mostly from the main sensor clusters. This type of record contains an early version of those fits, running from March 5, 0150, to March 5, 1208. The first 10 of the fits are to D-sensor data, with the remainder to C sensor data. The fits are always to five positive-ion species. Initially, the five species are H^+, S^{3+}, S^{2+}, O^+, and S^+, then S^{3+}, S^{2+}, O^+, S^+, and SO_2^+, then O^{2+}, S^{3+}, S^{2+}, S^+, SO_2^+, and finally O^{2+}, S^{3+}, S^{2+}, O^+, and S^+. Most of these fits assume equal thermal speeds for the species, although initially some assume equal temperatures. All assume equal velocities into the sensor, and the velocity component into the sensor is <u>not</u> a fit parameter. The velocity is taken to be either the rigid corotation value, or some fixed fraction thereof. The A array is defined as follows:

A(1):	cup number from which data taken
A(2):	number of positive-ion species fit (always 5)
A(3):	undefined flag
A(4):	undefined flag
A(5 → 9):	mass numbers of the five species
A(10→14):	charge numbers of the five species
A(15→19):	fit number densities of the five species
A(20→24):	fit thermal speeds of the five species
A(25→29):	velocity component into the sensor of the five species (all the same, not a fit parameter)
A(30):	fill

Caveats on Use: These fits are an early version of the final fits published by Bagenal and Sullivan (1981). They should provide good estimates of the total charge and mass densities in the torus, and qualitative estimates of temperatures. Relative composition should be disregarded, as these are not the final "best" fits (see Bagenal and Sullivan, 1981). Note that the seconds and minutes on the time array for this record type have been artificially set to zero. However, there will always be an adjacent (JMOD=2, JCAT=1) record on the tape, and this has the full time array.

G. Electron Moment and Fit Parameters (JMOD=3, JCAT=1)

These type of records give both moment and fit parameters for the electron spectra. Each record is an analysis of a composite spectrum using an E1 and an adjacent E2 spectrum. The time associated with the record is the time of the E1 spectrum. The answer array is defined as follows:

A(1): core fit density, #/cc

A(2): core fit temperature, eV

A(3): χ^2 for core fit

A(4): halo fit density, #/cc

A(5): halo fit temperature, eV

A(6): χ^2 for halo fit

A(7): s/c potential from fit

A(8): total fit density (sum of 1 and 4)

A(9): total fit temperature (density weighted average of 2 and 5)

A(10): moment density, #/cc (integration over observed distribution function)

A(11): moment temperature, eV (second moment of observed distribution function)

A(12): s/c potential from fits

A(13): angle between D-cup normal and magnetic field direction

A(14): angle between D-cup normal and s/c sun line

A(15): fill

A(16): estimate of total electron feed-through current (into positive ion mode) in main sensor due to fit electrons (halo + core), femtoamps

A(17): average energy of electron feed-through spectrum in main sensor, eV

A(18): inverse of the average of 1/energy of electron feed-through spectrum, in main sensor, eV.

A(19→21): same as 16 → 18, except for side sensor

A(22→24): same as 16 → 18, main sensor, except using moment density and temperature taken as a single Maxwellian to compute feed through (a bad approximation, useful for an upper limit estimate)

A(25→27): same as 22 →24, except for side sensor

A(28): ratio of core to halo feed-through current, side sensor

A(29): fill

A(30): fill

The electron feed-through contamination of the positive-ion estimate of N_+ (see III A) can be estimated by taking the total feed-through current, multiplying by 9.633×10^{-4} (9.179×10^{-4}) for the main (side) sensor, and dividing by V_n in km/sec (see equation 1 and the discussion in III A). This feed--through density then may be compared to the moment densities on this tape.

Caveats on Use: In addition to electron feed-through into the positive-ion mode, there is also the possibility of positive-ion feed-through into the electron modes. This will especially affect the suprathermal electrons when their density is less than ~1% of the core electrons. Since the importance of the suprathermals decreases with decreasing distance from the planet (Scudder et al. 1981), the suprathermals are therefore most strongly contaminated in the inner magnetosphere, especially in the Io torus inside of L ≃ 8. This effect is stronger inbound than outbound, because outbound the positive-ion flow is from the back of the D-sensor. Dr. Sittler at GSFC is currently rising the suprathermal analysis in the torus to eliminate this contamination, and any use of the current suprathermal analysis in the inner magnetosphere is discouraged pending his re-analysis. Outside of L ≃ 8, the suprathermal analysis is relatively unaffected by such feed-through. However, the suprathermal spectrum is almost never well-represented by a hot Maxwellian, and the present fits are under-estimates of the true suprathermal temperatures and densities when feed-through is unimportant.

Finally, in the Io torus itself (inside of L ≃ 8), the electron densities are systematically low by factors of order ten, because the spacecraft becomes negatively charged at high densities. The return current relationship used elsewhere in the magnetosphere is no longer valid, and as a result, the density estimates are low (see Scudder et al., 1981). There is also the possibility of a very cold electron component well below the PLS 10V threshold. Dr. Sittler at GSFC is currently working on improved temperature and density estimates in the torus.

IV. Description of the Tape

This is an IBM generated nine track binary tape. The Data Definition is:

```
DD UNIT=T1600,DCB=(RECFM=VBS,LRECL=1000,BLKSIZE=19069,DEN=4),
          LABEL=(1,BLP)
               =(2,BLP)
```

The Voyager 1 data are in the first file, and the Voyager 2 data are in the second file.

V. Bibliography

Bagenal, F., The Inner Magnetosphere of Jupiter and the Io Plasma Torus, Ph.D. Thesis, MIT, Cambridge, MA, June 1981.

Baganel, F., and J. D. Sullivan, Direct Plasma Measurements in the Io Torus and Inner Magnetosphere of Jupiter, J. Geophys. Res. 86 8447-8466, 1981.

Belcher, J. W., The Low-Energy Plasma in the Jovian Magnetosphere, in Physics of the Jovian Magnetosphere, A. J. Dessler, ed., Cambridge University Press, 1982.

Belcher, J. W. and R. L. McNutt, Jr., The Dynamic Expansion and Contraction of the Jovian Plasma Sheet, Nature 287, 813-815, 1980.

Belcher, J. W., C. K. Goertz, and H. S. Bridge, The Low Energy Plasma in the Jovian Magnetosphere, Geophys. Res. Lett. 7, 17-20, 1980.

Belcher, J. W., C. K. Goertz, J. D. Sullivan, and M. H. Acuña, Plasma Observations of the Alfven Wave Generated by Io, J. Geophys. Res. 86, 8508-8512, 1981.

Bridge, H. S., J. W. Belcher, A. J. Lazarus, A. M. Mavretic, J. D. Sullivan, G. L. Siscoe, and V.M. Vasyliunas, The Plasma Experiment on the 1977 Voyager Mission, Sp. Sci. Rev. 21, 259-287, 1977.

Bridge, H. S., J. W. Belcher, A., J. Lazarus, J. D. Sullivan, R. L. McNutt, Jr., F. Bagenal, J. D. Scudder, E. C. Sittler, G. L. Siscoe, V. M. Vasyliunas, C. K. Goertz, and C. M. Yeates, Plasma Observations Near Jupiter: Initial Results from Voyager 1, Science 204, 987-991, 1979.

Burlaga, L. F., J. W. Belcher, and N. F. Ness, Disturbances Observed Near Ganymede by Voyager 2, Geophys. Res. Lett. 7, 21-24, 1980.

Goodrich, C. C., J. D. Sullivan, and H. S. Bridge, Voyager Predictions of the Standoff Distance of the Jovian Bow Shock, MIT Report CSR-TR-80-4, June 1980.

McNutt, R. L., Jr., J. W. Belcher, J. D. Sullivan, F. Bagenal, and H. S. Bridge, Departure from Rigid Corotation of Plasma in Jupiter's Dayside Magnetosphere, Nature 280, 803, 1979.

McNutt, R. L. Jr., J. W. Belcher, and H. S. Bridge, Positive Ion Observations in the Middle Magnetosphere of Jupiter, J. Geophys. Res. 86, 8319-8342, 1981.

Scudder, J. D., E. C. Sittler, Jr., and H. S. Bridge, A Survey of the Plasma 86, 8157-8179, 1981.

Siscoe, G. L., A. Eviatar, R. M. Thorne, J. D. Richardson, F. Bagenal, and J. D. Sullivan, Ring Current Impoundment of the Io Plasma Torus, J. Geophys. Res. 86, 8480-8484, 1981.

Sullivan, J. D. and F. Bagenal, In situ identification of various ionic species in Jupiter's magnetosphere, Nature 280, 766, 1979.

Tokar, R. L., D. A. Gurnett, F. Bagenal, and R. R. Shaw, Light Ion Concentrations in Jupiter's Inner Magnetosphere, J. Geophys. Res., in press, 1982.

0 56366

F1 3/1/79 - 3/7/79

F2 7/4/79 - 7/12/79

RECORD 1 OF FILE 1
LENGTH = 7292 BYTES

7292	10	1979	60	12			474		
1C7C0000	00A00000	000007BB	0000003C	0000000C	00000001	00000000	000001DA	00000001	00000001
0000819C	424808EA	4127E36E	4292DB75	41400000	40D9C923	433625CF	3E76AB12	3E3E43B4	405F18ED
42140000	40266666	42102DB6	C013824F	40D13F7E	405FA530	7FFFFFFF	41C00000	7FFFFFFF	7FFFFFFF
7FFFFFFF	7FFFFFFF	7FFFFFFF	7FFFFFFF	7FFFFFFF	7FFFFFFF	7FFFFFFF	7FFFFFFF	7FFFFFFF	7FFFFFFF
7FFFFFFF	00A00000	000007BB	0000003C	0000000C	00000001	00000023	00000023	00000002	00000001
0000819C	42480737	4127EB24	42933469	41400000	40D9C438	43362412	3F2AAF5D	3EBB088F	4069FA60
42140000	40266666	42102DB6	3FAD8930	40949B93	40AF903A	7FFFFFFF	42390000	7FFFFFFF	7FFFFFFF
7FFFFFFF	7FFFFFFF	7FFFFFFF	7FFFFFFF	7FFFFFFF	7FFFFFFF	7FFFFFFF	7FFFFFFF	7FFFFFFF	7FFFFFFF
7FFFFFFF	00A00000	000007BB	0000003C	0000000C	00000002	00000007	000001B3	00000003	00000001
0000819C	405E1B03	412804CB	C11484E7	3F276FCC	4232CC09	404C7D8A	412DF686	405E1E03	413D4E60
405E0DCA	41EB5546	412DF637	427640BE	C14D53A0	7FFFFFFF	7FFFFFFF	7FFFFFFF	7FFFFFFF	7FFFFFFF
7FFFFFFF	7FFFFFFF	7FFFFFFF	7FFFFFFF	7FFFFFFF	7FFFFFFF	7FFFFFFF	7FFFFFFF	7FFFFFFF	7FFFFFFF
7FFFFFFF	00A00000	000007BB	0000003C	0000000C	00000002	00000024	000001DA	00000001	00000001
0000819C	424805E0	4127EAA1	4293D28A	41400000	40D9BC3D	43362243	3E6038DE	3E419414	40698C40
42140000	40266666	42102DB6	3FE3EDF0	405A2079	40CADEFF	7FFFFFFF	41800000	7FFFFFFF	7FFFFFFF
7FFFFFFF	7FFFFFFF	7FFFFFFF	7FFFFFFF	7FFFFFFF	7FFFFFFF	7FFFFFFF	7FFFFFFF	7FFFFFFF	7FFFFFFF
7FFFFFFF	00A00000	000007BB	0000003C	0000000C	00000003	0000000B	00000023	00000002	00000001
0000819C	424802D9	4127EA57	42942B7D	41400000	40D9CF95	433621DC	3F301A8E	3F116C8A	4079831D
42140000	40266666	42102DB6	40171085	4044653F	40D031A1	7FFFFFFF	423F0000	7FFFFFFF	7FFFFFFF
7FFFFFFF	7FFFFFFF	7FFFFFFF	7FFFFFFF	7FFFFFFF	7FFFFFFF	7FFFFFFF	7FFFFFFF	7FFFFFFF	7FFFFFFF
7FFFFFFF	00A00000	000007BB	0000003C	0000000C	00000003	0000002E	000001B3	00000003	00000001
0000819C	4073A0A6	4121063D	C1145143	3F234929	422A0613	409EA880	413D00F0	4073A0A6	412DD9C0
40738BD7	416E4366	413D011F	4260BF5B	C14DDDB0	7FFFFFFF	7FFFFFFF	7FFFFFFF	7FFFFFFF	7FFFFFFF
7FFFFFFF	7FFFFFFF	7FFFFFFF	7FFFFFFF	7FFFFFFF	7FFFFFFF	7FFFFFFF	7FFFFFFF	7FFFFFFF	7FFFFFFF
7FFFFFFF	00A00000	000007BB	0000003C	0000000C	00000004	0000000C	000001DA	00000001	00000001
0000819C	4248002C	4127E903	4294C99F	41400000	40D9DFBD	43362170	3E6E62CC	3E2FB182	40696A60
42140000	40266666	42102DB6	40127E49	40418103	40D24533	7FFFFFFF	41800000	7FFFFFFF	7FFFFFFF
7FFFFFFF	7FFFFFFF	7FFFFFFF	7FFFFFFF	7FFFFFFF	7FFFFFFF	7FFFFFFF	7FFFFFFF	7FFFFFFF	7FFFFFFF
7FFFFFFF	00A00000	000007BB	0000003C	0000000C	00000004	0000002F	00000023	00000002	00000001
0000819C	4247FE79	4127E989	42952292	41400000	40D9E8D6	4336210E	3F30A26A	3F119BC1	4079B7D9
42140000	40266666	42102DB6	3F902F90	405AF07B	40D6097C	7FFFFFFF	423D0000	7FFFFFFF	7FFFFFFF
7FFFFFFF	7FFFFFFF	7FFFFFFF	7FFFFFFF	7FFFFFFF	7FFFFFFF	7FFFFFFF	7FFFFFFF	7FFFFFFF	7FFFFFFF
7FFFFFFF	00A00000	000007BB	0000003C	0000000C	00000005	00000013	000001B3	00000003	00000001
0000819C	406E5FE6	41287580	C0640942	3F2751CB	4222793C	403697A6	41282909	406E5FE6	4134BD7B
406E5090	42334CDA	41282A1E	427432D8	C14E7690	7FFFFFFF	7FFFFFFF	7FFFFFFF	7FFFFFFF	7FFFFFFF
7FFFFFFF	7FFFFFFF	7FFFFFFF	7FFFFFFF	7FFFFFFF	7FFFFFFF	7FFFFFFF	7FFFFFFF	7FFFFFFF	7FFFFFFF
7FFFFFFF	00A00000	000007BB	0000003C	0000000C	00000005	00000030	000001DA	00000001	00000001
0000819C	4247FD22	4127E906	4295C083	41400000	40D9F92B	433621A9	3E7D2960	3E4B3694	40656E70
42140000	40266666	42102DB6	3FC65270	4058412E	40DB0C1D	7FFFFFFF	41E00000	7FFFFFFF	7FFFFFFF
7FFFFFFF	7FFFFFFF	7FFFFFFF	7FFFFFFF	7FFFFFFF	7FFFFFFF	7FFFFFFF	7FFFFFFF	7FFFFFFF	7FFFFFFF
7FFFFFFF	00A00000	000007BB	0000003C	0000000C	00000006	00000017	00000023	00000002	00000001
0000819C	4247FA1A	4127E8BC	429619A7	41400000	40D9F83C	43361F3F	3F2D81CF	3EE8CE5F	406FEE56
42140000	40266666	42102DB6	3F1FC470	408D7138	40C7F182	7FFFFFFF	42420000	7FFFFFFF	7FFFFFFF
7FFFFFFF	7FFFFFFF	7FFFFFFF	7FFFFFFF	7FFFFFFF	7FFFFFFF	7FFFFFFF	7FFFFFFF	7FFFFFFF	7FFFFFFF
7FFFFFFF	00A00000	000007BB	0000003C	0000000C	00000006	00000037	000001B3	00000003	00000001
0000819C	40690897	4131C6F5	C11183F9	3F26A3EE	42305C49	404A51C4	40932A41	40690897	4143917D
4068FFDE	4212E928	40932C11	427AEDC6	C14ECA40	7FFFFFFF	7FFFFFFF	7FFFFFFF	7FFFFFFF	7FFFFFFF
7FFFFFFF	7FFFFFFF	7FFFFFFF	7FFFFFFF	7FFFFFFF	7FFFFFFF	7FFFFFFF	7FFFFFFF	7FFFFFFF	7FFFFFFF
7FFFFFFF	00A00000	000007BB	0000003C	0000000C	00000007	00000018	000001DA	00000001	00000001
0000819C	4247F76F	4127E838	4296B7C8	41400000	40D9F213	43361CA6	3E603F8F	3E36B130	4069D383
42140000	40266666	42102DB6	BF381460	40A7C990	40BCF4C4	7FFFFFFF	41900000	7FFFFFFF	7FFFFFFF
7FFFFFFF	7FFFFFFF	7FFFFFFF	7FFFFFFF	7FFFFFFF	7FFFFFFF	7FFFFFFF	7FFFFFFF	7FFFFFFF	7FFFFFFF
7FFFFFFF	00A00000	000007BB	0000003C	0000000C	00000007	0000003B	00000023	00000002	00000001
0000819C	4247F5BA	4127E7EE	4297103B	41400000	40D9EEAD	43361B07	3F2D62EA	3EECC51B	4073251B
42140000	40266666	42102DB6	3F9A34D0	4098D02A	40C47BE7	7FFFFFFF	42450000	7FFFFFFF	7FFFFFFF
7FFFFFFF	7FFFFFFF	7FFFFFFF	7FFFFFFF	7FFFFFFF	7FFFFFFF	7FFFFFFF	7FFFFFFF	7FFFFFFF	7FFFFFFF
7FFFFFFF	00A00000	000007BB	0000003C	0000000C	00000008	0000001F	000001B3	00000003	00000001
0000819C	406E2D4C	412B837C	C020F331	3F2F7FFC	422B5ACB	4069292C	41149C38	406E2D4C	413E3471
406E7E83	421B7307	41149ACD	4278C00C	C14E69D0	7FFFFFFF	7FFFFFFF	7FFFFFFF	7FFFFFFF	7FFFFFFF
7FFFFFFF	7FFFFFFF	7FFFFFFF	7FFFFFFF	7FFFFFFF	7FFFFFFF	7FFFFFFF	7FFFFFFF	7FFFFFFF	7FFFFFFF
7FFFFFFF	00A00000	000007BB	0000003C	0000000C	00000009	00000000	000001DA	00000001	00000001
0000819C	4247F463	4127E76A	4297AEDC	41400000	40D9E8FA	43361973	3E8C9CAE	3E480827	4065D8DA
42140000	40266666	42102DB6	40110188	4086D1FC	40D3DA59	7FFFFFFF	41C00000	7FFFFFFF	7FFFFFFF
7FFFFFFF	7FFFFFFF	7FFFFFFF	7FFFFFFF	7FFFFFFF	7FFFFFFF	7FFFFFFF	7FFFFFFF	7FFFFFFF	7FFFFFFF
7FFFFFFF	00A00000	000007BB	0000003C	0000000C	00000009	00000023	00000023	00000002	00000001
0000819C	4247F159	4127E720	429807D0	41400000	40D9E63B	433616EE	3F2C7C28	3F109DE3	4071F658
42140000	40266666	42102DB6	BF581DE0	409791ED	40CEAF22	7FFFFFFF	42400000	7FFFFFFF	7FFFFFFF
7FFFFFFF	7FFFFFFF	7FFFFFFF	7FFFFFFF	7FFFFFFF	7FFFFFFF	7FFFFFFF	7FFFFFFF	7FFFFFFF	7FFFFFFF
7FFFFFFF	00A00000	000007BB	0000003C	0000000C	0000000A	00000007	000001B3	00000003	00000001
0000819C	4069F5D9	41270AF6	C06D6821	3F2ADD84	42201A3C	4050BF84	412A6E70	4069F5D9	413407B9
406A186E	4229CF89	412A6DC9	42769EB4	C14E10F0	7FFFFFFF	7FFFFFFF	7FFFFFFF	7FFFFFFF	7FFFFFFF
7FFFFFFF	7FFFFFFF	7FFFFFFF	7FFFFFFF	7FFFFFFF	7FFFFFFF	7FFFFFFF	7FFFFFFF	7FFFFFFF	7FFFFFFF
7FFFFFFF	00A00000	000007BB	0000003C	0000000C	0000000A	00000024	000001DA	00000001	00000001
0000819C	4247EEAC	4127E69C	4298A5F1	41400000	40D9E651	433614E3	3E94B833	3E3B4A57	4069AC28
42140000	40266666	42102DB6	BF20B3F0	40914B13	40CF3F70	7FFFFFFF	41A00000	7FFFFFFF	7FFFFFFF

7FFFFFFF	7FFFFFFF	7FFFFFFF	7FFFFFFF	7FFFFFFF	7FFFFFFF	7FFFFFFF	7FFFFFFF	7FFFFFFF	7FFFFFFF
7FFFFFFF	00A00000	000007BB	0000003C	0000000C	0000000B	0000000B	00000023	00000002	00000001
0000819C	4247ECFA	4127E652	4298FEE4	41400000	40D9E62F	4336139B	3F2AA830	3F104FF5	40702399
42140000	40266666	42102DB6	3F3864E0	40987BB8	40CE1BED	7FFFFFFF	423B0000	7FFFFFFF	7FFFFFFF
7FFFFFFF	7FFFFFFF	7FFFFFFF	7FFFFFFF	7FFFFFFF	7FFFFFFF	7FFFFFFF	7FFFFFFF	7FFFFFFF	7FFFFFFF
7FFFFFFF	00A00000	000007BB	0000003C	0000000C	0000000B	0000002B	000001B3	00000003	00000001
0000819C	406C82B9	4128A6AE	402913C3	3F2B3FF4	42317730	4072E0E0	4122864C	406C82B9	413C5DEE
406C86E1	421A2B4D	4122863B	4274C464	C14DD6C0	7FFFFFFF	7FFFFFFF	7FFFFFFF	7FFFFFFF	7FFFFFFF
7FFFFFFF	7FFFFFFF	7FFFFFFF	7FFFFFFF	7FFFFFFF	7FFFFFFF	7FFFFFFF	7FFFFFFF	7FFFFFFF	7FFFFFFF
7FFFFFFF	00A00000	000007BB	0000003C	0000000C	0000000C	0000000C	000001DA	00000001	00000001
0000819C	4247EBA2	4127E5CF	42999D05	41400000	40D9E61B	4336129A	3E76B528	3E547194	4069F5AF
42140000	40266666	42102DB6	BF74B170	408D23F1	40D5192D	7FFFFFFF	41B00000	7FFFFFFF	7FFFFFFF
7FFFFFFF	7FFFFFFF	7FFFFFFF	7FFFFFFF	7FFFFFFF	7FFFFFFF	7FFFFFFF	7FFFFFFF	7FFFFFFF	7FFFFFFF
7FFFFFFF	00A00000	000007BB	0000003C	0000000C	0000000C	0000002F	00000023	00000002	00000001
0000819C	4247E89A	4127E584	4299F5F8	41400000	40D9E63A	4336104F	3F2A5E5D	3EDCD12D	4077C877
42140000	40266666	42102DB6	3F688A40	4067FC12	40E15C2E	7FFFFFFF	423E0000	7FFFFFFF	7FFFFFFF
7FFFFFFF	7FFFFFFF	7FFFFFFF	7FFFFFFF	7FFFFFFF	7FFFFFFF	7FFFFFFF	7FFFFFFF	7FFFFFFF	7FFFFFFF
7FFFFFFF	00A00000	000007BB	0000003C	0000000C	0000000D	00000013	000001B3	00000003	00000001
0000819C	40731AFA	413403E8	C1192695	3F280F8E	42350764	40504EDB	C09CC337	40731AFA	4146789E
40730FBC	4223B5AA	C09CC0A2	426C1D21	C14D9570	7FFFFFFF	7FFFFFFF	7FFFFFFF	7FFFFFFF	7FFFFFFF
7FFFFFFF	7FFFFFFF	7FFFFFFF	7FFFFFFF	7FFFFFFF	7FFFFFFF	7FFFFFFF	7FFFFFFF	7FFFFFFF	7FFFFFFF
7FFFFFFF	00A00000	000007BB	0000003C	0000000C	0000000D	00000030	000001DA	00000001	00000001
0000819C	4247E5ED	4127E500	429A9419	41400000	40D9F15D	43360F60	3E558F3A	3E374DA0	406988E9
42140000	40266666	42102DB6	4021624E	40649387	40DF3E6A	7FFFFFFF	41900000	7FFFFFFF	7FFFFFFF
7FFFFFFF	7FFFFFFF	7FFFFFFF	7FFFFFFF	7FFFFFFF	7FFFFFFF	7FFFFFFF	7FFFFFFF	7FFFFFFF	7FFFFFFF
7FFFFFFF	00A00000	000007BB	0000003C	0000000C	0000000E	00000017	00000023	00000002	00000001
0000819C	4247E43C	4127E436	429AED0D	41400000	40D9F73B	43360EB5	3F261E9E	3EDA7DAB	40797E4D
42140000	40266666	42102DB6	BF808D70	408F089A	40CEF15B	7FFFFFFF	42430000	7FFFFFFF	7FFFFFFF
7FFFFFFF	7FFFFFFF	7FFFFFFF	7FFFFFFF	7FFFFFFF	7FFFFFFF	7FFFFFFF	7FFFFFFF	7FFFFFFF	7FFFFFFF
7FFFFFFF	00A00000	000007BB	0000003C	0000000C	0000000E	00000037	000001B3	00000003	00000001
0000819C	4074A9AF	412818D1	C0845551	3F223249	423AAECD	405918EF	411FB9FE	4074A9AF	41394C52
40749774	4216CC98	411F3A2D	42779600	C14E1770	7FFFFFFF	7FFFFFFF	7FFFFFFF	7FFFFFFF	7FFFFFFF
7FFFFFFF	7FFFFFFF	7FFFFFFF	7FFFFFFF	7FFFFFFF	7FFFFFFF	7FFFFFFF	7FFFFFFF	7FFFFFFF	7FFFFFFF
7FFFFFFF	00A00000	000007BB	0000003C	0000000C	0000000F	00000018	000001DA	00000001	00000001
0000819C	4247E2E5	4127E432	429B882E	41400000	40DA02CE	43360ECE	3E60345A	3E3D411C	406965D1
42140000	40266666	42102DB6	BF681AD0	40A91BCA	40C3EAF3	7FFFFFFF	41900000	7FFFFFFF	7FFFFFFF
7FFFFFFF	7FFFFFFF	7FFFFFFF	7FFFFFFF	7FFFFFFF	7FFFFFFF	7FFFFFFF	7FFFFFFF	7FFFFFFF	7FFFFFFF
7FFFFFFF	00A00000	000007BB	0000003C	0000000C	0000000F	0000003B	00000023	00000002	00000001
0000819C	4247DFDB	4127E3E8	429BE421	41400000	40DA0A08	43360D3C	3F2DA506	3F13526A	4070E69F
42140000	40266666	42102DB6	C01AF39E	40BEDDDA	40B0A277	7FFFFFFF	42410000	7FFFFFFF	7FFFFFFF
7FFFFFFF	7FFFFFFF	7FFFFFFF	7FFFFFFF	7FFFFFFF	7FFFFFFF	7FFFFFFF	7FFFFFFF	7FFFFFFF	7FFFFFFF
7FFFFFFF	00A00000	000007BB	0000003C	0000000C	00000010	0000001F	000001B3	00000003	00000001
0000819C	4066A422	412846ED	40592E9E	3F269737	422C4238	40997C5C	4129F714	4066A422	4138EAF1
4066BB53	4243CC3B	4129F697	42834E47	C14E8840	7FFFFFFF	7FFFFFFF	7FFFFFFF	7FFFFFFF	7FFFFFFF
7FFFFFFF	7FFFFFFF	7FFFFFFF	7FFFFFFF	7FFFFFFF	7FFFFFFF	7FFFFFFF	7FFFFFFF	7FFFFFFF	7FFFFFFF
7FFFFFFF	00A00000	000007BB	0000003C	0000000C	00000011	00000000	000001DA	00000001	00000001
0000819C	4247DD2F	4127E364	429C8242	41400000	40D9F95E	43360995	3EC20568	3E3F3301	4066309C
42140000	40266666	42102DB6	BFD35B10	40C4ED7E	40A8BE5C	7FFFFFFF	41C00000	7FFFFFFF	7FFFFFFF
7FFFFFFF	7FFFFFFF	7FFFFFFF	7FFFFFFF	7FFFFFFF	7FFFFFFF	7FFFFFFF	7FFFFFFF	7FFFFFFF	7FFFFFFF
7FFFFFFF	00A00000	000007BB	0000003C	0000000C	00000011	00000023	00000023	00000002	00000001
0000819C	4247DB7E	4127E31A	429CDB35	41400000	40D9F012	43360762	3F2F49D1	3F1331A0	407121F2
42140000	40266666	42102DB6	3F6B8E30	408EA922	40CF06DD	7FFFFFFF	423E0000	7FFFFFFF	7FFFFFFF
7FFFFFFF	7FFFFFFF	7FFFFFFF	7FFFFFFF	7FFFFFFF	7FFFFFFF	7FFFFFFF	7FFFFFFF	7FFFFFFF	7FFFFFFF
7FFFFFFF	00A00000	000007BB	0000003C	0000000C	00000012	00000007	000001B3	00000003	00000001
0000819C	4076D2BF	41274D50	C0A9091B	3F248033	42210BED	408C958D	411DDB30	4076D2BF	41317413
4076DFB4	421C0EFC	411DDAF8	42719936	C14D9D70	7FFFFFFF	7FFFFFFF	7FFFFFFF	7FFFFFFF	7FFFFFFF
7FFFFFFF	7FFFFFFF	7FFFFFFF	7FFFFFFF	7FFFFFFF	7FFFFFFF	7FFFFFFF	7FFFFFFF	7FFFFFFF	7FFFFFFF
7FFFFFFF	00A00000	000007BB	0000003C	0000000C	00000012	00000024	000001DA	00000001	00000001
0000819C	4247DA26	4127E296	429D7956	41400000	40D9DFA5	433604C0	3E483C4B	3E2B0F46	4069B946
42140000	40266666	42102DB6	3F171610	4099089C	40D07256	7FFFFFFF	41800000	7FFFFFFF	7FFFFFFF
7FFFFFFF	7FFFFFFF	7FFFFFFF	7FFFFFFF	7FFFFFFF	7FFFFFFF	7FFFFFFF	7FFFFFFF	7FFFFFFF	7FFFFFFF
7FFFFFFF	00A00000	000007BB	0000003C	0000000C	00000013	0000000B	00000023	00000002	00000001
0000819C	4247D71D	4127E24B	429DD249	41400000	40D9E139	4336029D	3F277CA1	3EBFDB8C	40802911
42140000	40266666	42102DB6	4013BDDE	40976197	40CE3DE5	7FFFFFFF	423F0000	7FFFFFFF	7FFFFFFF
7FFFFFFF	7FFFFFFF	7FFFFFFF	7FFFFFFF	7FFFFFFF	7FFFFFFF	7FFFFFFF	7FFFFFFF	7FFFFFFF	7FFFFFFF
7FFFFFFF	00A00000	000007BB	0000003C	0000000C	00000013	0000002B	000001B3	00000003	00000001
0000819C	4075B25E	4123E3F3	C0428A3F	3F2BF884	423D6212	4063CAF7	40D03A80	4075B25E	4142DAA1
4075A7B1	421B054A	40D03CAC	4276D218	C14DC8E0	7FFFFFFF	7FFFFFFF	7FFFFFFF	7FFFFFFF	7FFFFFFF
7FFFFFFF	7FFFFFFF	7FFFFFFF	7FFFFFFF	7FFFFFFF	7FFFFFFF	7FFFFFFF	7FFFFFFF	7FFFFFFF	7FFFFFFF
7FFFFFFF	00A00000	000007BB	0000003C	0000000C	00000014	0000000C	000001DA	00000001	00000001
0000819C	4247D46F	4127E1C7	429E706A	41400000	40D9F2D4	43360253	3E79FC3D	3E575A33	4069F229
42140000	40266666	42102DB6	3F9C2E40	4084F575	40D47335	7FFFFFFF	41B00000	7FFFFFFF	7FFFFFFF
7FFFFFFF	7FFFFFFF	7FFFFFFF	7FFFFFFF	7FFFFFFF	7FFFFFFF	7FFFFFFF	7FFFFFFF	7FFFFFFF	7FFFFFFF
7FFFFFFF	00A00000	000007BB	0000003C	0000000C	00000014	0000002F	00000023	00000002	00000001
0000819C	4247D2BC	4127E17D	429EC95D	41400000	40D9FCB1	43360206	3F260538	3EBE8B54	407E21F7
42140000	40266666	42102DB6	4012FA93	40A5C609	40C4E1E9	7FFFFFFF	423F0000	7FFFFFFF	7FFFFFFF
7FFFFFFF	7FFFFFFF	7FFFFFFF	7FFFFFFF	7FFFFFFF	7FFFFFFF	7FFFFFFF	7FFFFFFF	7FFFFFFF	7FFFFFFF
7FFFFFFF	00A00000	000007BB	0000003C	0000000C	00000015	00000013	000001B3	00000003	00000001
0000819C	40745B3E	4131A883	C0267291	3F24CD21	423C017F	4014696E	C04BEF43	40745B3E	4144A30E
40744442	41A96CE5	C043E392	4276C28A	C14E7690	7FFFFFFF	7FFFFFFF	7FFFFFFF	7FFFFFFF	7FFFFFFF
7FFFFFFF	7FFFFFFF	7FFFFFFF	7FFFFFFF	7FFFFFFF	7FFFFFFF	7FFFFFFF	7FFFFFFF	7FFFFFFF	7FFFFFFF
7FFFFFFF	00A00000	000007BB	0000003C	0000000C	00000015	00000030	000001CA	00000001	00000001
0000819C	4247D161	4127E0F9	429F677E	41400000	40DA0E58	433602C0	3E70508B	3E3BF300	4068746C